J Mater Sci (2008) 43:5823–5836
DOI 10.1007/s10853-008-2877-6

# Hybrid organic–inorganic materials based on polypyrrole and 1,3-dithiole-2-thione-4,5-dithiolate (DMIT) containing dianions

**Antonio Gerson Bernardo da Cruz · James Lewis Wardell · Ana M. Rocco**

Received: 31 March 2008 / Accepted: 14 July 2008 / Published online: 31 July 2008


**Abstract** The synthesis of hybrid materials by electropolymerization of pyrrole and inorganic complexes based on the DMIT ligand (1,3-dithiole-2-thione-4,5-dithiolate), e.g. $[NEt_4]_2[M(DMIT)_n]$ (M = Ni, Pd or Pd, $n = 2$; M = Sn, $n = 3$], in acetonitrile solution is reported. Spectroscopic data showed that DMIT-containing anions, $[M(DMIT)_n]^{2-}$, were inserted into the polypyrrole framework without chemical modification during the electropolymerization process. Cyclic voltammetry showed that materials obtained were electroactive, undergoing redox processes related to both the conducting polymer and the counteranions. The electrochemical results also suggest that, in the case of the transition metal containing films, the counteranions are not trapped in the PPy matrix but undergo anion exchange during the redox cycle of PPy. However, an opposite behaviour was observed with the film with $[M(DMIT)_n]^{2-}$. The films exhibit good thermal stabilities and have conductivity values expected for semiconductors. This study of these hybrid materials highlights the importance of targeting specific materials for specific applications.

A. G. B. da Cruz (✉)
Departamento de Física e Química/ICE, Universidade Federal de Itajubá (UNIFEI), Itajuba, MG, Brazil
e-mail: gerson.bernardo@unifei.edu.br

J. L. Wardell
Departamento de Química, Universidade Federal de Minas Gerais (UFMG), Belo Horizonte, MG, Brazil

A. M. Rocco
Grupo de Materiais Condutores e Energia, Departamento de Processos Inorgânicos, Escola de Química, Universidade Federal do Rio de Janeiro (UFRJ), Rio de Janeiro, RJ, Brazil

## Introduction

Nanostructured conducting polymers and their composites have emerged as a new field of research and development, directed to the creation of smart materials for use in modern and future technologies. The main applications for nanostructured conducting polymers are as electric energy storage systems, sensors and biosensors and anti-corrosion materials [1].

Conducting polymers for practical applications require high intrinsic conductivities as well as good chemical and physical stabilities. Polypyrrole (PPy) satisfies these conditions and is one of the most extensively studied conducting polymers [2–20], in such areas as electrode materials (batteries and "supercapacitors" [3], polymer electrolytes [4], protective films (against a static electricity or a microwave irradiation) [5], anti-corrosion protection [6, 7], separating membranes for gases and liquids [8], sensors and biosensors [9], actuators and artificial muscles [10], micro- and nanoelements for the information storage and transformation [11, 12], (electro)luminescent materials, "smart windows" and solar energy conversion [13], electrochromic media [14, 15], catalysis and electrocatalysis (catalyst support for the PEM type fuel cells) [16, 17], optoelectronics [18] and bioelectronics [19]. Moreover these materials provide a demanding challenge to the accepted knowledge of charge transport processes [20].

Polypyrrole can be synthesized chemically or electrochemically. Electrochemical synthesis of polymers directly onto an electrode surface offers some advantages over chemical synthesis. Electrochemical synthesis allows the uniform deposition of insoluble polymer films onto irregular surfaces with controlled thicknesses and with better adherence than in the case of chemically synthesized conducting polymers. The chemical modification of

electrode surfaces by electrically generated polymeric pyrrole films containing active centres, especially inorganic metal complexes, is a convenient way of obtaining hybrid organic–inorganic materials with particular functions. These modifications present opportunities for the design of eclectic materials by taking advantage of the best properties of their components.

The hybrid concept goes beyond this approach, by creating materials with novel structures or supramolecular architectures with synergic properties or even with activities not present in the individual components. Studies of electrode modification by polypyrrole, electrochemically synthesized with complex counteranions of transition metals, have already been reported [21]. Linear $[Au(CN)_2]^-$, square planar $[Ni(CN)_4]^{2-}$ and other anionic species [22] have been incorporated in PPy frameworks. These materials were obtained in order to study the relationship between the anion structures and the physical properties of the PPy material. Studies of such systems can give valuable information about the effects on the polymer arrangement, which is intrinsically related to the counteranion structure [23, 24].

In our laboratory, we have pursued in recent years the design of electroactive hybrid materials based on electronically conducting organic polymers (ECP) and electroactive inorganic species containing the 1,2-dithiolate ligand, 1,3-dithiole-2-thione-4,5-dithiolate, $[C_3S_5]^{2-}$, $[DMIT]^{2-}$,[1] Fig. 1, foreseeing possible applications in the field of materials science [25–29]. Compounds containing these heterocyclic dianions have been the subject of a substantial amount of research, which has been facilitated by the efficient synthesis of $[DMIT]^{2-}$ by alkali metal reduction of carbon disulphide [30, 31]. The prime interest in these anions is as precursors of electronic and photonic materials [32]. Coordination complexes of $[DMIT]^{2-}$, especially certain salts of $[M(DMIT)_2]^{n-}$ ($M = Ni$ and Pd and $0 < n < 2$), have metal-like conductivity and at least eight $[M(DMIT)_2]^{n-}$ salts ($M = Ni$, Pd) have been found to be superconductors [33].

In the present work, we report results on electropolymerized polypyrrole hybrid films with DMIT containing counteranions $(PPy/[M(DMIT)_m]^{2-}$ [$M = Ni$, Pd or Pt, $n = 2$; $M = Sn$, $n = 3$]. The films have been characterized by spectroscopic, morphological, electrochemical, electrical and thermal techniques. The modifications of electrodes with these hybrid materials (organic conducting polymer/DMIT complexes) are fundamentally interesting for solid-state science, opening up new perspectives in inorganic chemistry, materials science, nanoscience and nanotechnology due to their potential application in the design of molecular electronic devices [34, 35]. Furthermore these electrodes can serve as analytical sensors or as reference electrodes. Such modifications are designed to control the behaviour of the electrode/solution interface [36].

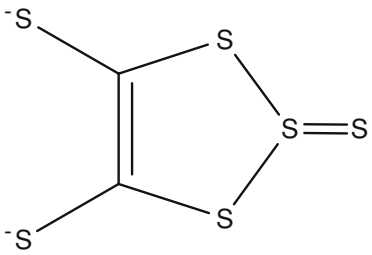

**Fig. 1** The 1,3-dithiole-2-thione-4,5-dithiolate (DMIT) dianion

## Experimental

### Materials

Pyrrole and acetonitrile were obtained from Aldrich. Pyrrole was distilled under vacuum prior to use and stored at −5 °C. All other reagents and solvents were of analytical grade and were used without further purification.

### Synthesis of tetraethylammonium-based DMIT complexes

$[Et_4N]_2[Zn(DMIT)_2]$ was synthesized according to a published procedure [30]. **$[Et_4N]_2[Ni(DMIT)_2]$**: A solution containing $[Et_4N]_2[Zn(DMIT)_2]$ (1.0 mmol) and $NiCl_2 \cdot 6H_2O$ (1.0 mmol) in methanol was stirred overnight at room temperature. The dark green solid was filtered off and recrystallized from methanol yielding 86%.

A similar procedure was used in the syntheses of **$[Et_4N]_2[Pd(DMIT)_2]$** and **$[Et_4N]_2[Pt(DMIT)_2]$** from $PdCl_2$ (1.0 mmol) and $K_2[PtCl_4]$ (1.0 mmol), respectively. The resulting brown and black solids were collected by filtration and recrystallized from methanol yielding 78 and 88% for the Pd and Pt complexes, respectively.

**$[Et_4N]_2[Sn(DMIT)_3]$:** Solutions of $SnCl_4 \cdot 5H_2O$ (1.0 mmol) in $H_2O$ (10 mL) and $[Et_4N]_2[Zn(DMIT)_2]$ (1.5 mmol) in acetone (30 mL) were mixed and stirred for 24 h at room temperature. The orange solid was filtered off, washed with isopropanol and methanol and vacuum-dried. The sample was recrystallized from acetone yielding 86%.

### Electrodes preparation

Before polymerization, the Pt electrodes were polished with 0.3 μm $Al_2O_3$ powder and rinsed thoroughly with

[1] The acronym 'DMIT' stems from the name *dimercaptoisotrithione*, an older nomenclature system for sulphur-based heterocycles.

water, cleaned in a sonication bath, and dried. The FTO electrodes were cleaned in a sonication bath successively with acetone (10 min) and water (10 min). The substrates were then immersed in a $H_2O/H_2O_2$ (30%)/$NH_3$ (25%) (5:1:1 v/v) mixture for 30 min. The substrates were then washed with water and dried.

### Electropolymerization of the hybrid films

The hybrid films, PPy/$[Ni(DMIT)_2]^{2-}$ (**I**), PPy/$[Pd(DMIT)_2]^{2-}$ (**II**), PPy/$[Pt(DMIT)_2]^{2-}$ (**III**) and PPy/$[Sn(DMIT)_3]^{2-}$ (**IV**), were grown in a one-compartment electrochemical glass cell (volume, 10.0 mL) with platinum electrodes (working and counter electrodes) each having an area of 2.5 $cm^2$. Fluorine/tin oxide glass (FTO) was also used as the working electrode. All the potentials reported in this paper are referenced to that of the saturated calomel electrode (SCE). Hybrid films of polypyrrole with the DMIT-based counteranions were synthesized from pyrrole (0.1 mol $L^{-1}$) and $[Et_4N]_2[M(DMIT)_m]$ (0.005 mol $L^{-1}$) in acetonitrile ($CH_3CN$), at room temperature. The electrochemical cell was purged with ultra-pure argon, prior to polymerization, and the argon atmosphere was maintained over the solution throughout the synthesis. The chemically modified electrodes were obtained under galvanostatic and potentiodynamic conditions. Under galvanostatic conditions, a constant current density ($j$) of 0.15 mA $cm^{-2}$ was applied for 8 min, which corresponds to a synthesis charge ($Q_s$) of 72 mC $cm^{-2}$. Under potentiodynamic condition, successive sweeps ranging from −1000 to 1000 mV with a scan rate of 100 mV $s^{-1}$ were used. An Autolab PGSTAT 30 potentiostat/galvanostat controlled by GPES (General Purpose Electrochemical System) software was used in all electrochemical experiments. All the hybrid films were rinsed in $CH_3CN$ and dried under vacuum before analysis.

### Characterization

FTIR spectra with a resolution of 4.0 $cm^{-1}$ were obtained using a Nicolet 760 Magna-IR spectrometer in CsI discs. The electronic spectra (UV–vis) of the solutions were obtained with a HP845A diode array spectrophotometer.

The surface morphology of the electrodeposited hybrid films was analysed by scanning electron microscopy with a JEOL JSM-840A scanning electron microscope operating at an acceleration voltage of 20.0 kV. The analysed hybrid films were grown on fluorine/tin oxide electrodes (2.5 $cm^2$). The samples were mounted in aluminium plates and coated with a gold dispersion.

Electrochemical experiments were carried out using an Autolab PGSTAT 30 potentiostat/galvanostat. Cyclic voltammetric experiments were carried out at 50 mV $s^{-1}$ in a one-compartment electrochemical glass cell (volume, 10 mL) under ultra-pure argon atmosphere using a Pt electrode covered with the hybrid films as working electrode, a platinum foil as auxiliary electrode and a saturated reference calomel electrode (SCE). All the experiments were carried out in acetonitrile solutions with $NaBF_4$ (0.1 mol $L^{-1}$) as the supporting electrolyte.

Conductivities ($\sigma$) of the films deposited on the fluorine/tin oxide glass electrodes were obtained as mean values of ten measurements at room temperature using a HP-34420A nanovoltimeter/microohmimeter connected to a linear four-probe system.

Thermal gravimetric analyses (TGA) of hybrid films were carried out using a TGA50 Shimadzu instrument with a heating rate of 10 °C $min^{-1}$ from room temperature up to 800 °C in aluminium pans under a nitrogen atmosphere.

## Results and discussion

### Electropolymerization of hybrid films

The process that transforms insulating polymers to excellent conductors is the formation of charge-transfer complexes with electron donors (n-doping, reduction) or electron acceptors (p-doping, oxidation). The doped polymer backbone becomes negatively or positively charged with the dopant forming oppositely charged ions (doping).

The polymerization is initiated by an oxidation step, followed by radical cation formation, coupling reaction, deprotonation, and a one-electron oxidation in order to regenerate the aromatic system. The most decisive, however, are the current density and the electrolyte, particularly the anion nature because it is incorporated into the polymer as a counterion. In general, one anion is incorporated for every three pyrrole units.

The chronopotentiometric curves for the electropolymerization of hybrid films under galvanostatic conditions (Fig. 2) show that all reactions follow an instantaneous nucleation regime.

From previous studies on the polymer growth by Abrantes et al. [37] and from the characteristic growth depicted in Fig. 2, it was possible to define three different polymerization stages:

- From A to B the diffusion controlled monomer oxidation in solution takes place;
- From B to C there is a diffusion controlled nucleation of oligomers produced in solution;
- From C to D the overlap of growing centres takes place.

The movement of species in solution, which accompanies this process, is due to diffusion and migration, resulting in the displacement of monomeric species

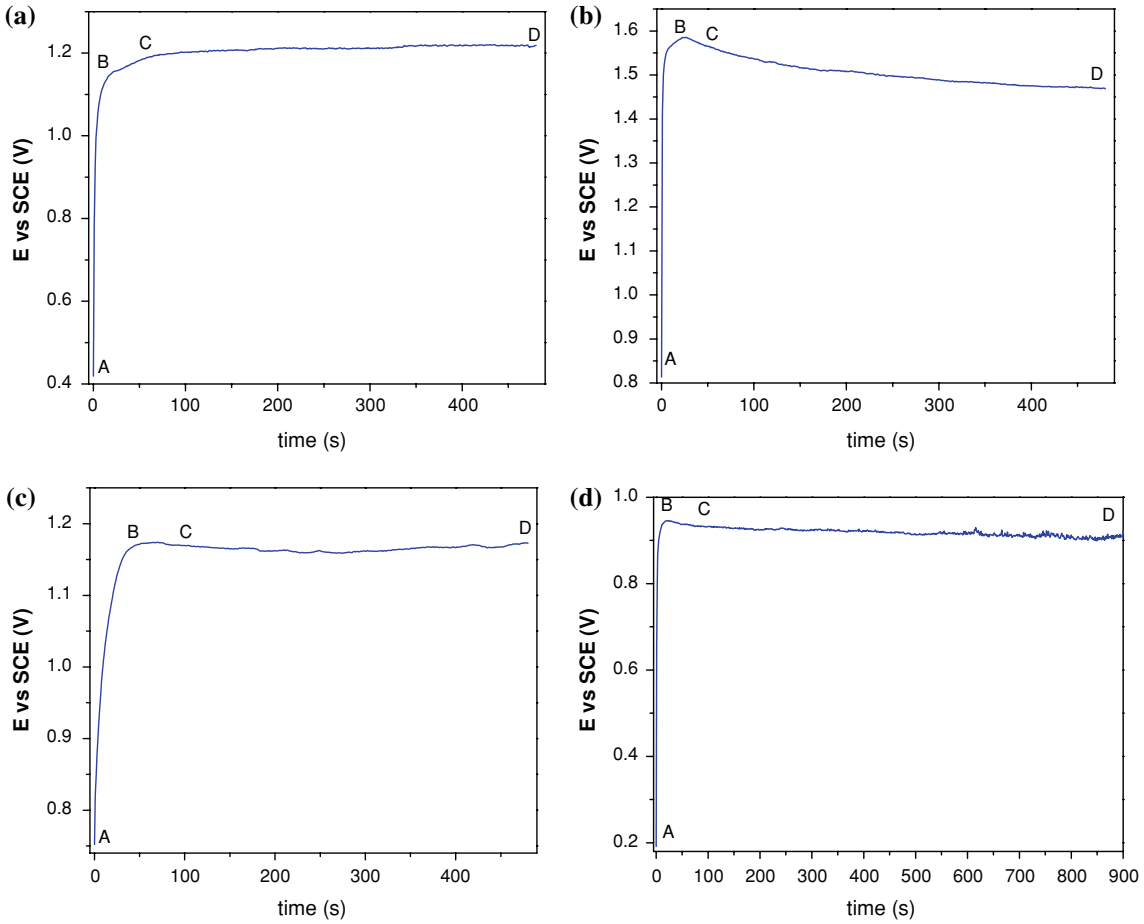


**Fig. 2** Chronopotentiometric curve obtained during the galvanostatic electropolymerization of a 0.1 mol $L^{-1}$ Py and 0.005 mol $L^{-1}$ (**a**) $[NEt_4]_2[Ni(DMIT)_2]$, (**b**) $[NEt_4]_2[Pd(DMIT)_2]$, (**c**) $[NEt_4]_2[Pt(DMIT)_2]$ and (**d**) $[NEt_4]_2[Sn(DMIT)_3]$ acetonitrile solution in Pt electrode to obtaining the hybrid films. Current density = 0.15 mA $cm^{-2}$

towards the electrode surface (A–B). After B the movement of the protons, formed during the pyrrole oxidation away from the electrode, must also be accounted for as soon as a polymer is formed and oxidized at the surface (C). In this system, flux of other species is expected, such as anion diffusion and drift towards the electrode for polymer charge compensation or non-consumed oligomers away from its surface.

Figure 3 shows the curves for the conducting polymer hybrid film formation on the Pt electrode surface as the thickness increases with successive potential cycles. The thin film growth was observed after the 3rd potential sweep cycle and a high adherent coloured film was deposited on the electrode surface. The cyclic voltammograms show broad oxidation-reduction peaks during the electropolymerization of the hybrid films. During the process, an increase in current response was observed for almost all polymers, except for the film IV, which showed a decrease in the current response suggesting that a low conductive material had been deposited on the electrode surface.

The doping kinetics of the process is dependent on the nature of the counteranion, particularly its size, which influences its mobility in the polymer chain. During the electropolymerization, a small number of electrons are removed from the polymer chains in response to the positive applied potential, creating a net positive charge on the polymer and thus establishing an electric field. The resulting positively charged "holes" (polarons and bipolarons) move away from the electrode along the polymer chains by drift (due to an electric field, also known as migration) and diffusion (due to a concentration gradient). The polymer backbone must be locally linear for the polymer to accept and conduct these positive charge carriers. At the same time, anions in the electrolyte move towards the polymer surface in response to the electric field through a combination of drift and diffusion (depletion of the ions in the electrolyte may render their concentration so low that drift is not negligible in the solution). The ions enter the polymer and then move through the polymer, between the chains, by a combination of drift and diffusion. Space between the polymer

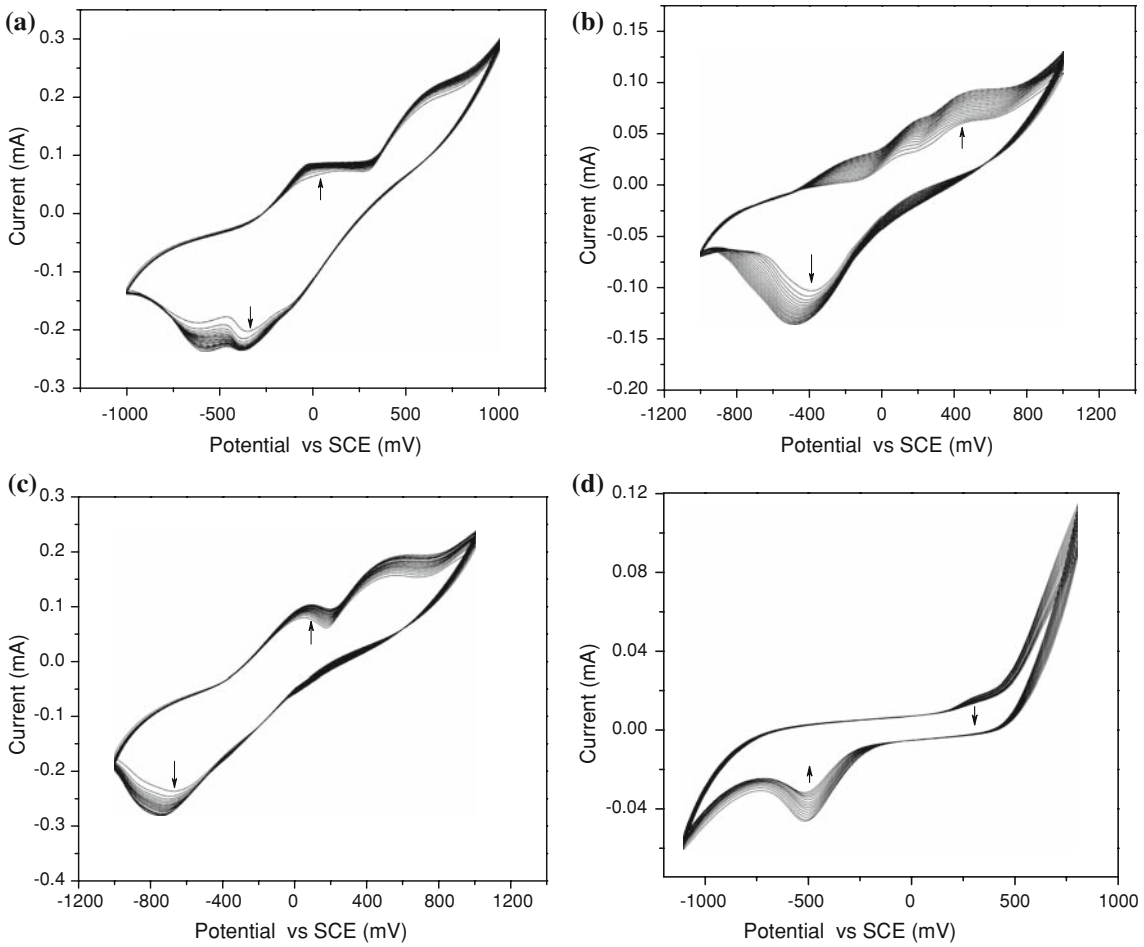


**Fig. 3** Consecutive cyclic voltammograms obtained during the electropolymerization of a 0.1 mol $L^{-1}$ Py and 0.005 mol $L^{-1}$ (**a**) $[NEt_4]_2[Ni(DMIT)_2]$, (**b**) $[NEt_4]_2[Pd(DMIT)_2]$, (**c**) $[NEt_4]_2[Pt(DMIT)_2]$ and (**d**) $[NEt_4]_2[Sn(DMIT)_3]$ acetonitrile solution to obtaining the hybrid films. Pt foil as working electrode and $\upsilon = 100$ mV $s^{-1}$

chains must be created in order for the ions to be accommodated; hence the ion current depends on chain movements as well as on the degree of polymer solvation, ion size, ion-polymer interactions, and related features.

Previous infrared, X-ray photoelectron (XPS) and NMR spectroscopic studies of PPy have established that the polymer contains several types of defects, which cause a deviation from chain linearity [38]. Some of these are illustrated in Fig. 4.

Overoxidation is a major source of chemical defects and occurs when the anodic potential is higher than the oxidation potential of the polymer [38]. The overoxidation of PPy is an inevitable consequence of film growth in the presence of nucleophiles since the oxidation potential of PPy is lower than that of pyrrole. Aliphatic groups are believed to be produced through the addition of hydrogen to the pyrrole ring under the acidic conditions of electropolymerization. Coupling through the $\beta$ position of the pyrrole ring is also likely to be an important source of structural defects. The presence of non-alternating pyrrole rings will cause a deviation from chain linearity. It is clear that chemical and structural defects have a significant influence on the PPy properties, which are sensitive to structural order and charge transport.

Pure PPy films and the hybrid films grown in acetonitrile from FTO substrates and Pt substrates were submitted to a peel test using 3M® adhesive tape in order to evaluate the adherence to the electrode substrate. PPy/M(DMIT) hybrid films remain strongly bound to the substrate, in contrast to PPy alone. According to Simon et al. and Collard et al., such adhesion differences can be attributed to different nucleation and growth modes [39, 40]. In agreement with the observations of Saunders et al. [38] and Takakubo et al. [41], the thickness of the films was found to increase with increasing depth in the electrolyte solution. This effect has been attributed to current density variations at the electrode surface. Hence, the conductivities should be measured at several different sections of the films corresponding to regions of the maximum and minimum depths in the solution, and at intermediate positions.

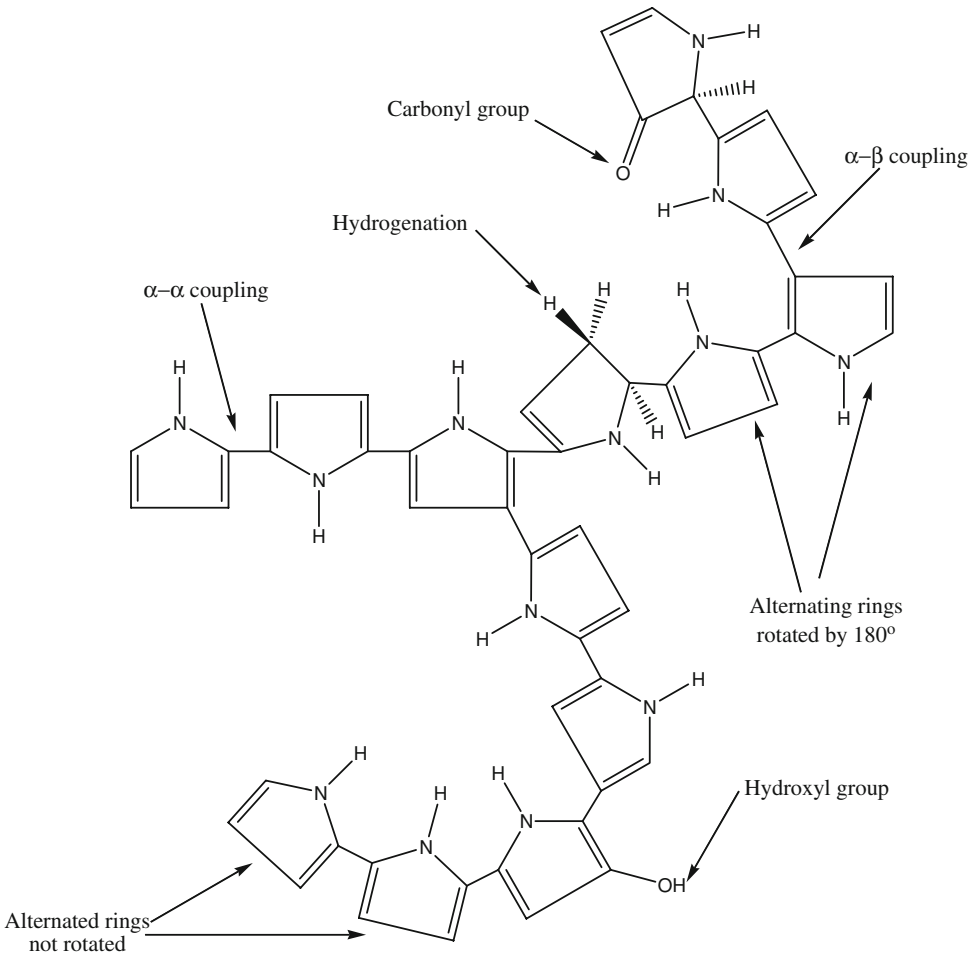


**Fig. 4** Diagram showing various defects in the structure of polypyrrole

## Spectroscopic characterization

FTIR spectra of the $[NEt_4]_2[M(DMIT)_n]$ complexes are shown in Fig. 5. The anions exhibit C=C displacement out of plane bands [ca. 1030 $cm^{-1}$], S–C–S + C=S stretches [ca. 900 $cm^{-1}$] and C=C stretch [ca. 1400 $cm^{-1}$] [42–45]. The bands in the region of 3000–2900 $cm^{-1}$ and the low intensity bands at 1490, 1100 and 784 $cm^{-1}$ are assigned to the tetraethylammonium cation.

FTIR spectrum of pure PPy is shown in Fig. 6a with characteristic bands at 3400, 1550, 1470, 1280–1030, 787 and 671 $cm^{-1}$, which are assigned as N–H stretching vibrations, pyrrole ring stretch, conjugated C–N stretching, =C–H in plane deformation and C–H outer-bending vibrations, respectively [46]. A strong band at 1700 $cm^{-1}$ is also observed and arises from C=O formation, indicating some degree of overoxidation of PPy chains [46].

The FTIR spectra of the hybrid films I–IV are depicted in Fig. 6. Bands in the region of 1030 and 1058 $cm^{-1}$, corresponding to C=C displacement out of plane and S–C–S + C=S stretching, respectively, are clearly visible in the spectra of the PPy/M-DMIT hybrid films. Changes however are observed in the form, intensity and wavenumber of some bands assigned to the original complex dianion. As reported for other PPy/complex counteranions, a broad absorption band was observed above 1800 $cm^{-1}$ for all films. This band has been attributed to free charge carriers, arising from interchain excitations [38]. The characteristic absorption bands of polypyrrole were observed at 1560, 1470, 1280 and 784 $cm^{-1}$. The expected PPy bands in the region of 1030–1100 $cm^{-1}$ are overlapped by DMIT vibrations, e.g. bands assigned to the ring deformation C–H stretching and C–N deformation in the region of 1030 $cm^{-1}$ are masked by the bands assigned to C = S stretching observed in the region of 960–1060 $cm^{-1}$. The disappearance of the asymmetric NH stretch at 3400 $cm^{-1}$ in PPy indicates interaction between the N–H and the DMIT-containing moieties. A similar behaviour was observed by Cervini et al. with PPy/$[Ni(CN)_4]^{2-}$ films [47].

Observation of these spectral bands confirms the incorporation of the unmodified counteranions.

## Morphological characterization

Scanning electron micrographs of the fluorine/tin oxide glass electrodes coated with hybrid films are shown in

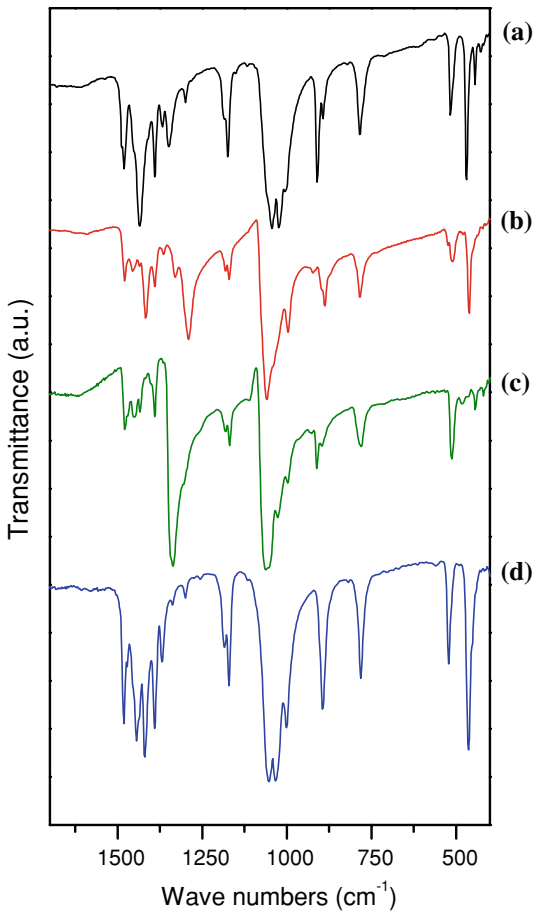


**Fig. 5** FTIR spectra in transmission mode of the (a) $[NEt_4]_2[Ni(DMIT)_2]$, (b) $[NEt_4]_2[Pd(DMIT)_2]$, (c) $[NEt_4]_2[Pt(DMIT)_2]$ and (d) $[NEt_4]_2[Sn(DMIT)_3]$ complexes. CsI discs

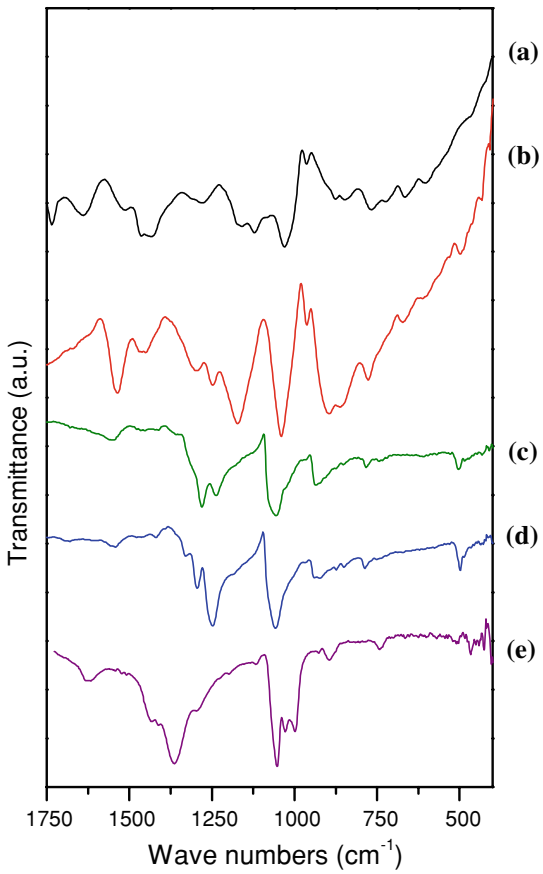


**Fig. 6** FTIR spectra in transmission mode of the (a) pure PPy, (b) PPy/$[Ni(DMIT)_2]^{2-}$, (c) PPy/$[Pd(DMIT)_2]^{2-}$, (d) PPy/$[Pt(DMIT)_2]^{2-}$ and (e) PPy/$[Sn(DMIT)_3]^{2-}$ hybrid films. CsI discs

Fig. 7. As is shown, various morphologies such as island-type, semispheroid, spheroid (cauliflower) and needle-like are present.

The surface of the hybrid films I, II and III, are irregular with inhomogeneities. Step formation with dominant needle-like structures can be identified, see Fig. 7a–c, which indicate a two-dimensional growth with fibrous and semi-spheroid structures similar to those found for PPy/$[ClO_4^-]$ and PPy/$[BF_4^-]$. The semispheroid structures, on the other hand, suggest a three-dimensional growth. The lack of a uniform distribution indicates that preferential growth sites are located in the fibres.

Compared to hybrid films I, II and III the morphology of film IV is more homogeneous. From Fig. 7d, island type structures are identified, which are distributed on a regular and homogeneous surface. Cauliflower structures (Fig. 7d insert) are revealed by cracks after days of exposure to air. These structures emerge from the bulk of the film. Two explanations for this phenomenon are plausible. Exposure to oxygen can cause a degradation of the hybrid film. Saunders et al. [38] reported that PPy hybrid films with bulky counteranions, such as tetrasulphonated metallophthalocyanines, [M(TSPC)], suffer attack by atmospheric $O_2$ causing irreversible covalent bond formation of oxygenated species at the film surface. Alternatively, the cracks arise from relaxation of the octahedral structure of the $[Sn(DMIT)]^{2-}$ counteranion. This relaxation will result in the polymer chains attaining a low energy conformation.

The morphologies observed for the hybrid films depend on the counteranion and may result in the PPy film undergoing different mechanisms of nucleation and growth.

## Electrochemical characterization

Cyclic voltammograms, shown in Fig. 8a–d, were obtained from the Pt electrode covered with the PPy-DMIT hybrid films in acetonitrile solutions containing 0.1 mol $L^{-1}$ $NaBF_4$. For all hybrid films, stable voltammograms were observed after the two initial cycles.

The films I, II and III exhibited electrochromism ranging from dark green to greenish yellow in colour. During the initial cathodic cycle, a very sharp and intense peak

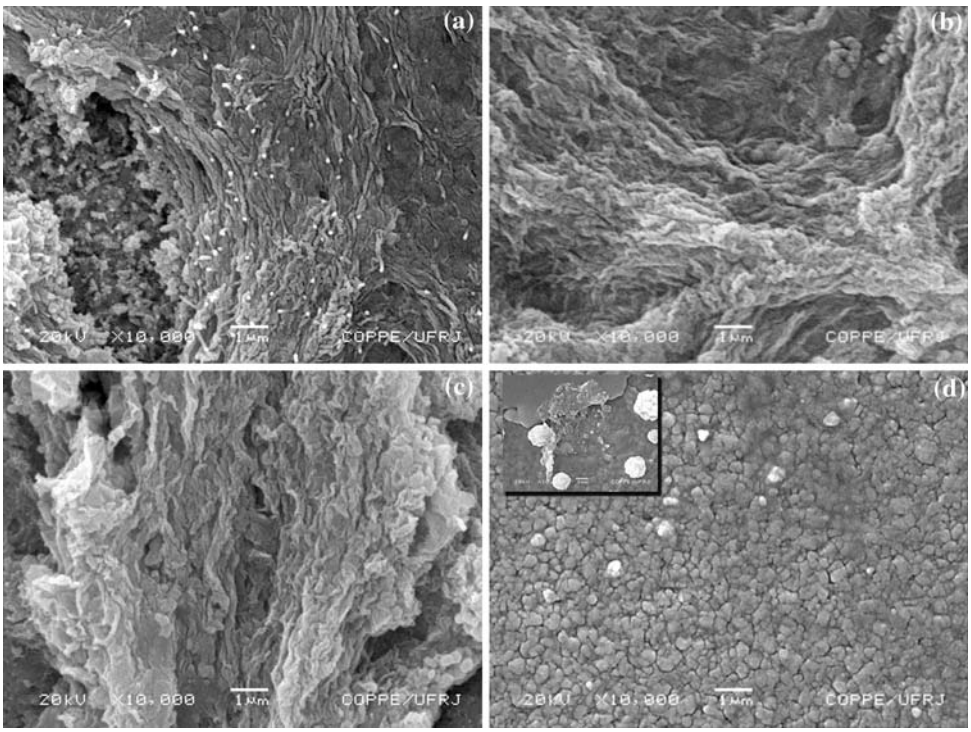


**Fig. 7** Scanning electron photomicrographs of fluorine/tin oxide glass electrodes covered with the galvanostatically electropolymerized (**a**) PPy/$[Ni(DMIT)_2]^{2-}$, (**b**) PPy/$[Pd(DMIT)_2]^{2-}$, (**c**) PPy/$[Pt(DMIT)_2]^{2-}$ and (**d**) PPy/$[Sn(DMIT)_3]^{2-}$ hybrid films

between 500 and 800 mV was observed. A coloured gradient is formed around the working electrode along with this electrochemical reduction. In the first anodic voltammogram, large anodic peaks are observed at 200, 100 and 130 mV, corresponding to the polymer redox processes for films I, II and III, respectively. The second cathodic scan shows only one peak, whose intensity decreases on subsequent cycles (no colour gradient was observed from this point).

The peaks for the hybrid film IV, in the potential range responsible for the oxidation-reduction of the polypyrrole, are somewhat sharper compared to those of the other hybrid films and those with classical counteranions [48]. This indicates that the redox behaviour is obscured by the capacitive charging waves that characterize polymers doped with complex counteranions [49].

The half wave potential values, $E_{1/2}$, of the hybrid films were calculated as the average of the anodic and cathodic peak potentials ($Ep_a$ and $Ep_c$, respectively). The $\Delta Ep$ values ($Ep_a - Ep_c$) characterize an irreversible redox process. According to Li et al. [50], Cheung et al. [51] and Cervini et al. [47], who found similar cyclic voltammogram shapes to those in Fig. 8a–c using other PPy-counteranion systems, a useful measure of reversibility in cyclic voltammograms of conducting polymers is the peak current ratio $Ip_a/Ip_c$. Under ideal conditions, this ratio would be unity. For the systems under study, the values obtained are in the range of 0.4–0.8, increasing with subsequent sweeps. The cathodic current decreases and the reduction wave broadens, but the oxidation wave remains almost unchanged. The oxidation and reduction reactions cause spatial distortions in the chains, which is partly responsible for the broad redox waves shown in Fig. 8a–d. According to Cervine et al. and Dong et al. [47, 52], such distortions probably occur in two stages. In the first stage (reduction), cations are incorporated into the polymer and form ion pairs with the mobile anions, while in the second stage these ion pairs and the surplus anions diffuse out of the film. In this way, a concentration gradient is set up inside the film.

The above-mentioned behaviour was not observed for film IV [29]. The observed peaks for the hybrid film IV are narrow and their width increased with potential sweeping. No electrochromism and dissolution were observed during the cathodic sweep for the hybrid film IV. For the other hybrid films (I–III), the decreasing current was attributed to distortion in the film structure due to the compressional effect, which is caused by the doping/de-doping of the species. For film IV, however, the current increases with increasing number of cycles. This fact points to a cation ($Na^+$) interchange (doping/de-doping) during the cycling in order to keep the electro-neutrality of the film. This suggests that $[Sn(DMIT)_3]^{2-}$ units are trapped into the polymer matrix and cannot be released during the oxidation of PPy. In the hybrid films with Ni(TSPC), studied by Varela et al. [53], the counteranions are not involved in the doping and de-doping of the anions from the polymeric matrix as the charge compensation process is assigned to the movement of the positive charged species. This behaviour was also

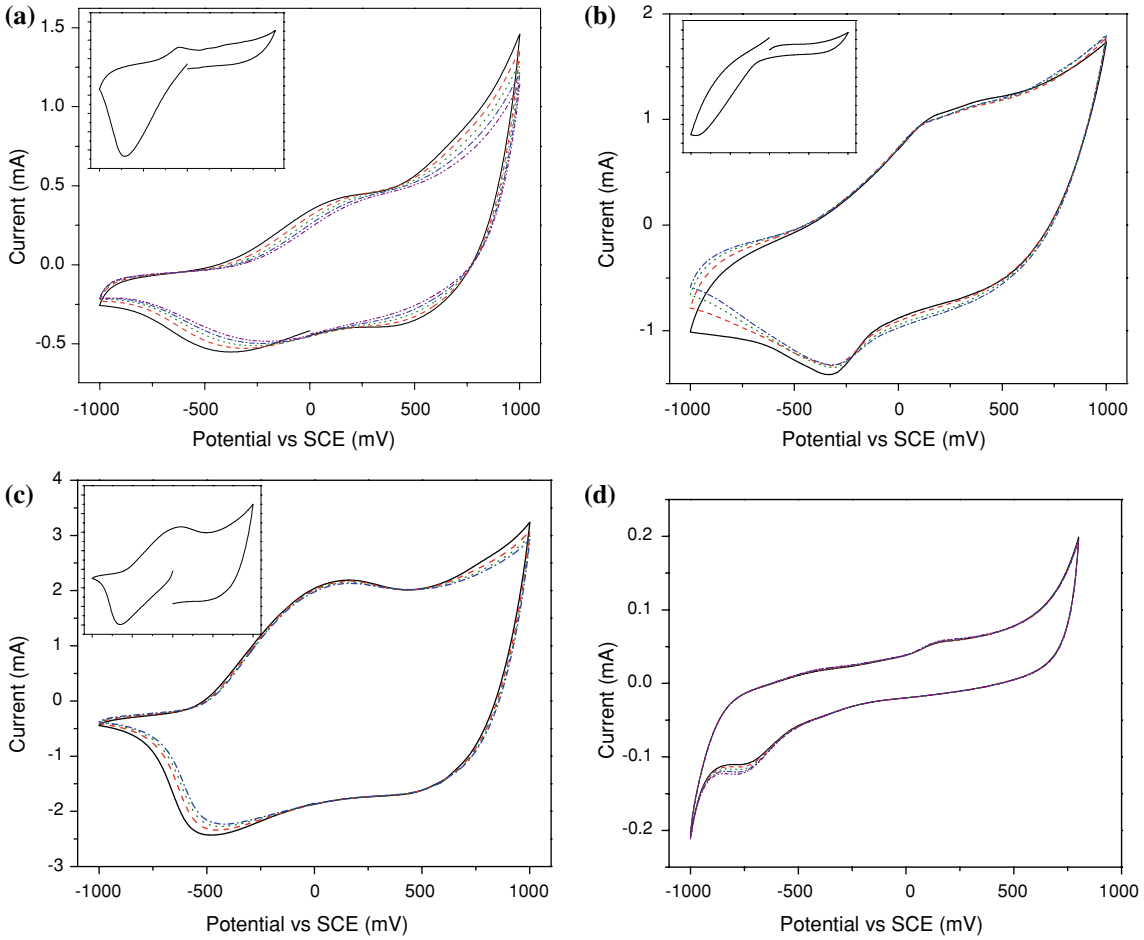


**Fig. 8** Consecutive cyclic voltammograms obtained for the (**a**) PPy/$[Ni(DMIT)_2]^{2-}$, (**b**) PPy/$[Pd(DMIT)_2]^{2-}$, (**c**) PPy/$[Pt(DMIT)_2]^{2-}$ and (**d**) PPy/$[Sn(DMIT)_3]^{2-}$ hybrid films in $NaBF_4$ 0.1 mol $L^{-1}$ acetonitrile solution. Pt foil as working electrode and $\upsilon = 50$ mV $s^{-1}$. In the inserted graphs are shown the sharp electrodissolution peaks in the initials cathodic cycles

observed for other systems [54–56] and may also arise with the hybrid film IV. The phenomenon may be related with the volume occupied by the $[Sn(DMIT)_3]^2$. Previous studies using $[Bi(DMIT)_2]^-$ as the counter anion in hybrid films with PPy showed a similar result [28].

The sharp initial charge peak, observed for each of the hybrid films I, II and III, is related to an electro-dissolution process involving the counteranions and pyrrole oligomers [57]. The subsequent continuous changes can be attributed to a progressive interchange of the $[M(DMIT)_2]^{2-}$ anions from the films with $BF_4^-$ anions from solution. In order to check this hypothesis, the resultant solutions were evaluated by UV–vis spectroscopy.

Figure 9 shows the UV–vis spectrum obtained from a solution obtained after cyclic voltammetry (oxidation/reduction cycles). The main absorptions of the DMIT complexes are present in the spectra [26–29, 31], which suggest that partial de-doping of the film with expulsion of $[M(DMIT)_2]^{2-}$ anions (M = Ni, Pd and Pt) takes place during the reduction process. During the potential cycles, the current response of the redox peaks of hybrid films, I-III, decreases with increases in the scan number up to the fifth cycle, formal potential of the cathodic peaks shifts positively and the peak current decreases. In the following five cycles, the two pairs of peaks become ill-defined and the response current decreases continuously. This phenomenon can be explained as follows. The two redox peaks observed in the initial cycles are related to the polypyrrole oxidation and reduction along with the doping or de-doping of the electrolyte ions ($Na^+$ and $BF_4^-$). The redox reaction of polypyrrole is $PPy^0 \leftrightarrow (PPy)^{n+} + ne^-$. In this way, the electroneutrality of the film is guaranteed in the oxidized state of PPy ($PPy^{n+}$). During the reduction stage the process of the reduction of the positive charges should be accompanied by the insertion of $Na^+$ into the film to compensate for the negatively charged $[M(DMIT)_2]^{2-}$. On the other hand, the $[M(DMIT)_2]^{2-}$ is slowly released from the film during the potential cycling. Consequently, as the positive charge in the PPy chains cannot be fully compensated by the remaining $[M(DMIT)_2]^{2-}$, $BF_4^-$ ions

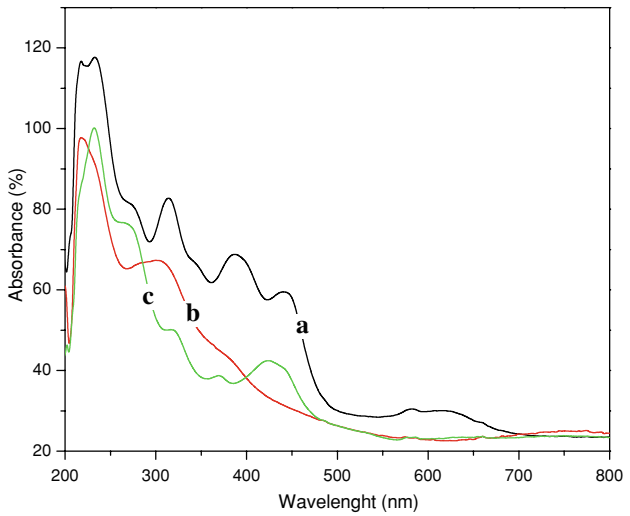


**Fig. 9** Absorption spectra obtained for the solutions $NaBF_4$ in acetonitrile after 10 potential sweeping of the (a) PPy/$[Ni(DMIT)_2]^{2-}$, (b) PPy/$[Pd(DMIT)_2]^{2-}$ and (c) PPy/$[Pt(DMIT)_2]^{2-}$ hybrid films

inserts into the film to maintain the electroneutrality. The smaller the quantity of $[M(DMIT)_2]^{2-}$ retained, the larger the number of $BF_4^-$ ions needed. Thus, from cycle to cycle, the main counteranions involved in the process changes progressively from $Na^+$ to $BF_4^-$ ions. Consequently, the insertion of the spherical $BF_4^-$ ions into the film results in a compressional effect, which distorts the film structure and leads to broadening of the two peaks and a decreased current [57]. This hypothesis was confirmed by the UV–vis spectra obtained from the solutions after the voltammetric experiments (Fig. 9).

As a summary of the electrochemical results, hybrid films I, II and III undergo dissolution process during the first cathodic sweeping and are electrochromic. The DMIT-based anions are not trapped into polymeric matrix. Film IV does not show electrochromism and the $[Sn(DMIT)_3]^{2-}$ anion seems to be trapped into the polymeric matrix. This fact suggests that the electroneutrality inside this film is maintained by the doping/de-doping of cations instead of anions. Table 1 summarizes the electrochemical data.

## Doping level ($\delta$) estimation

The doping level ($\delta$), defined as the measure of the polymer oxidation (or reduction), is given by the ratio between the charge of the polymer and the number of monomeric units in the polymer chain.

The polypyrrole film formation can be expressed by:

$$(n+2)RH_2 - (2n+2)e^- \rightarrow HR{-}Rn{-}RH + (2n+2)H^+$$

When $n$ is large, two Faradays per mol are required for bond formation (in the case of a linear polymer). In order to transform the polymer to the oxidized form (doped), an extra quantity is required.

$$HR{-}Rn{-}RH - (n+2)\delta e^- + (n+2)\delta A^- \rightarrow (HR{-}Rn{-}RH) + (n+2)\delta A - (n+2)\delta$$

where $\delta$ has values between 0.1 and 0.4. The doping level characterizes the polymer, especially in relation to charge storage.

To estimate the doping level, the Bobacka's relation was used [58] with the data obtained from the cyclic voltammograms of the hybrid films. In order to estimate the doping level some assumptions have to be made: The polymerization efficiency was taken to be 100%, and the measured charge during the synthesis ($Q_t$) was equivalent to the synthesis charge $Q_s = \psi Q_t$ and $Q_s = n(2 + \delta)$, with $n$ equal to the polymerized monomeric units. The electrochemical response of the polymeric film, $Q_r$, was defined as half the charge required in the oxidation and reduction processes; $Q_r = n\delta F$, obtained by integration of the area under the voltammetric peak. These assumptions, and the use of the equation below, gave an estimated doping level for hybrid films which is listed in Table 2.

$$\delta = \frac{2Q_r}{Q_s - Q_r} \quad (1)$$

The values suggest a high counteranion incorporation and is in agreement with values reported by Cervini et al. [47] and Takakubo et al. [41] for PPy/$[Ni(CN)_4]^{2-}$ and

**Table 1** Electrochemical data obtained from the cyclic voltammograms of the PPy/$[M(DMIT)_m]^{n-}$ hybrid films

| Films | Ep (mV) | $E_{1/2}$ (mV) | ΔEp (mV) | $I$ (mA) | $Ip_a/Ip_c$ |
|---|---|---|---|---|---|
| PPy/$[Ni(DMIT)_2]^{2-}$ | 200 a | −135 | 730 | 0.70 a | 0.8 |
| | −530 c | | | −0.90 c | |
| PPy/$[Pd(DMIT)_2]^{2-}$ | 100 a | −110 | 420 | 0.30 a | 0.4 |
| | −320 c | | | −0.70 c | |
| PPy/$[Pt(DMIT)_2]^{2-}$ | 130 a | −330 | 920 | 1.10 a | 0.6 |
| | −790 c | | | −1.70 c | |
| PPy/$[Sn(DMIT)_3]^{2-}$ | 137 a | −296 | 867 | 0.10 a | 0.4 |
| | −730 c | | | −0.02 c | |

a: anodic; c: cathodic

**Table 2** Estimated doping levels for the PPy/$[M(DMIT)_m]^{n-}$ hybrid films

| Films | $Q_s$ (mC) | $Q_r$ (mC) | $\delta$ |
|---|---|---|---|
| PPy/$[Ni(DMIT)_2]^{2-}$ | 72.0 | 16.9 | 0.27 |
| PPy/$[Pd(DMIT)_2]^{2-}$ | 72.0 | 13.0 | 0.20 |
| PPy/$[Pt(DMIT)_2]^{2-}$ | 72.0 | 27.4 | 0.47 |
| PPy/$[Sn(DMIT)_3]^{2-}$ | 90.0 | 2.01 | 0.04 |

$Q_s$: synthesis charge; $Q_r$: reduction charge

PPy/$[Cr(ox)_3]^{3-}$ films. These values can be compared to those found for PPy/Co(TSPC) [38] and PPy/$[Au(CN)_2]^-$ films [59]. However, the lower value obtained for the film IV follows a tendency observed by Saunders for PPy/$[FeEDTA]^-$ hybrid films. A mean value of 0.059 was reported by the author and was attributed to the lower charge of the counteranion.

Saunders et al. [38] observed that the ratio of the incorporated counteranion to pyrrole units decreases both with the increasing size and charge of the counteranion. However, these two tendencies do not seem to be responsible for the obtained doping level values. These values may be related to the anion mobility within the polymer chain, which would facilitate its incorporation as well as the PPy capacity to self-adjust to an optimized doping level. Increasing the volume of the counteranion seems to be responsible for the lower value of $\delta$ observed for the hybrid film IV.

## Thermal stability

Figure 10 shows the TGA curves for the hybrid films. In the thermal decomposition of hybrid films, II and III, an initial mass loss due to evaporation of residual solvent or absorbed water was observed at about 80 °C. This step reveals that these films are highly porous retaining solvent or environmental water within the polymer chains. Thermal decompositions associated with the metallic complex counteranions were observed in the range of 150–350 °C. Two other events occur in the range of 350–520 and 520–800 °C. These latter decompositions involve polypyrrole degradations with cleavage of high molar mass products such as oligomers and dimers [60].

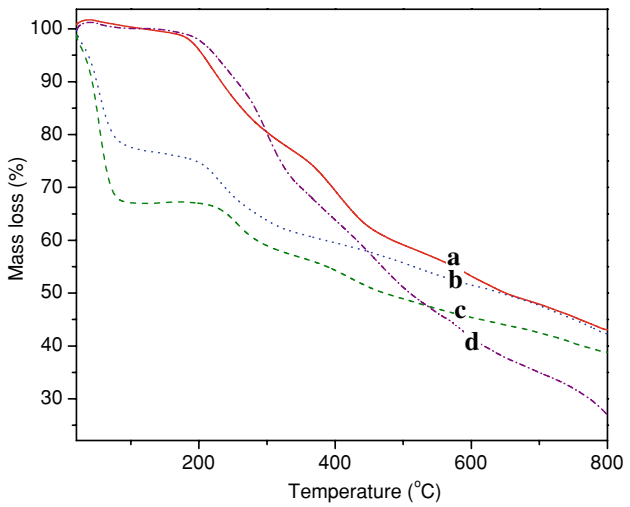


**Fig. 10** Thermogravimetric curves of the (**a**) PPy/$[Ni(DMIT)_2]^{2-}$, (**b**) PPy/$[Pd(DMIT)_2]^{2-}$, (**c**) PPy/$[Pt(DMIT)_2]^{2-}$ and (**d**) PPy/$[Sn(DMIT)_3]^{2-}$ hybrid films

Thermal decomposition of film IV begins at 200 °C and occurs in six steps.

All the hybrid films, I–IV, exhibit higher thermal stabilities than does that of PPy/DDS (DDS = dodecylsulphate) and arise from the good thermal stabilities of the complex counteranions rather than PPy. As an example of the thermal stabilities of salts of the complex anions, we can mention that the thermal decomposition of $[NEt_4]_2[Sn(DMIT)_3]$ begins at 210 °C [29]. The decomposition kinetics of the films are affected by the inserted counteranion. Lower decomposition rates are found for the films than for the isolated tetraethylammonium salts of the complex counteranions [61]. The thermal stability data obtained from TGA curves are summarized in Table 3.

## Conductivity measurements

A variety of units can be used to describe the efficiency of charge transport in an ECP sample. In principle, there are two different quantities that can describe this efficiency. One can talk either about the conductivity or the resistivity of an ECP. When referring to the resistivity of an ECP, often the *volume resistivity* or *bulk resistivity*, $\rho_v$, is used. The S.I. unit of the volume resistivity is $\Omega\ m^{-1}$, but in the literature this resistivity is usually given in $\Omega\ cm^{-1}$. The volume resistivity is defined as the resistance between opposite faces of a unit cube. To characterize the current flow over a surface, the *sheet resistivity*, $\rho_s$, is often used. The surface resistivity is frequently used to characterize current flow over a film surface and is defined as the resistance between opposite edges of an unit square. The sheet resistivity is independent of the size of the square and its unit is simply the Ohm. The sheet resistivity is not a material property, but only a property of a specific specimen. Sheet resistivity is usually given in $\Omega^{-1}$. Conductivity is defined as the reciprocal resistivity. The unit of conductance, the reciprocal Ohm, is usually called Siemens (S).

The sheet resistivity measurements ($\rho_s$) were carried out with a fluorine/tin oxide glass electrode ($10\ \Omega^{-1} < \rho_s < 20\ \Omega^{-1}$) covered with the polymeric film, using colinear four probe geometry [62].

It is well known that the *sheet resistivity* is a more precise measurement when dealing with films deposited on insulators. The problem with evaluating sheet resistivity of films deposited on highly conductive substrates is the underlying assumption that electrons move from the negative electrode across the top surface of the conductive layer only to the positive layer. This implies that you cannot measure sheet resistivity of the films on highly conductive substrates. For these reasons, correction factors related to the conductive bottom boundary and geometries were used in order to minimize the effect of conductive substrate in the obtained sheet resistivity values [32–35].

**Table 3** Stages, temperatures ranges, $DTG_{(max)}$ and weight loss data for the PPy/$[M(DMIT)_m]^{n-}$ hybrid films

| Films | Decomposition step | Temperature range (°C) | Peak temperature DTG (°C) | Mass loss (%) |
|---|---|---|---|---|
| PPy/$[Ni(DMIT)_2]^{2-}$ | **I** | 17–170 | 80.0 | 2.4 |
| | **II** | 170–360 | 219.8 | 21.6 |
| | **III** | 360–510 | 400.9 | 19.3 |
| | **IV** | 510–670 | 592.4 | 9.8 |
| | **V** | 670–800 | 755.3 | 5.8 |
| PPy/$[Pd(DMIT)_2]^{2-}$ | **I** | 17–150 | 53.5 | 32.3 |
| | **II** | 150–350 | 256.7 | 10.1 |
| | **III** | 350–520 | 420.9 | 17.9 |
| | **IV** | 520–800 | 755.0 | – |
| PPy/$[Pt(DMIT)_2]^{2-}$ | **I** | 18–145 | 53.3 | 23.3 |
| | **II** | 145–380 | 230.1 | 15.9 |
| | **III** | 380–610 | 524.2 | 8.9 |
| | **IV** | 610–800 | 781.2 | 8.8 |
| PPy/$[Sn(DMIT)_3]^{2-}$ | **I** | 20–110 | 53.4 | 1.1 |
| | **II** | 110–250 | 232.4 | 8.8 |
| | **III** | 250–350 | 296.9 | 21.5 |
| | **IV** | 350–590 | 453.9 | 25.8 |
| | **V** | 590–660 | 595.5 | 6.8 |
| | **VI** | 660–800 | 798.8 | 13.3 |

The volume conductivity, $\sigma_v$, and correction factors were calculated using the following equation [63–65]:

$$\sigma_v = \frac{\pi}{\ln(2)} w \left(\frac{V}{I}\right) f_{12} f_{2R} \quad (2)$$

where $\sigma_v$ is the volume conductivity, $w$ is the film thickness (cm), $V$ is the potential drop between the inner probes (V), $I$ is applied current in the outer probes (A) and $f_{12}$ and $f_{2R}$ are correction factors.

The film thickness ($w$) was estimated using the relation of Wernet and Wegner [66]:

$$w = \frac{Q_s}{2FA\phi}\left(\frac{m_1 + m_2}{\delta}\right) \quad (3)$$

where $Q_s$ is the synthesis charge used during the electropolymerization, $F$ is the Faraday constant ($9.6485 \times 10^7$ mC/mol), $\phi$ is the density of the material (considered to be = 1.1 g/cm$^3$), $m_1$ is the molar mass of the pyrrole unit, $m_2$ is the molar mass of the counteranion and $\delta$ is the number of pyrrole units per counteranion.

The correction factor $f_{12}$ is defined as:

$$f_{12} = \frac{\ln(2)}{\left[\frac{\cosh(w/s)}{\cosh(w/2s)}\right]} \quad (4)$$

where $f_{12}$ is the finite thickness correction factor and $s$ is the spacing between the probes (0.119 cm).

The estimation of the thickness by this approach has two flaws:

1. The actual volume occupied by a metal site in the polymer systems should be larger than that predicted from the above, due to the size of unit and the packing of the polymer which should result in a larger average unit size.
2. Polymer swelling: Film swelling on the uptake of electrolyte solutions is a well-known and important phenomenon. The degree of swelling can vary from around 15 to 180% for non-polar aprotic polymers, and as much as one hundred-fold for a protonated polar polymer. The process is critical for the introduction of the counterions necessary to maintain electroneutrality and also for the creation of the free volume through which these ions may move. This point is further complicated by changes in the swelling concomitant with changes in the oxidation state of the redox active sites. Neither is considered in the present calculation of the thickness.

It is clear from point (1) that the true concentration of the dianion should be lower than expected, which, from Eq. 3, would entail a thickness larger than expected, and the swelling considered in point (2) will make the thickness even larger still. These errors in $w$ imply that calculated conductivity values will have some error, but they will underestimate the true value.

Conductivity values obtained for hybrid films are in the range expected for semiconductors and appear to depend on the geometry of the incorporated counteranion. Yamaura

**Table 4** Thickness, $f_{12}$ and $f_{2R}$ correction factors and conductivity values for the PPy/$[M(DMIT)_m]^{n-}$ hybrid films

| Films | Thickness, $w$ (μm) | $f_{12} = \frac{\ln(2)}{\left[\frac{\cosh(w/s)}{\cosh(w/2s)}\right]}$ | $f_{2R}$ | Conductivity (S/cm) |
|---|---|---|---|---|
| PPy/$[Ni(DMIT)_2]^{2-}$ | 2.1 | 5889.7 | 0.9313 | $2.2 \times 10^{-3}$ |
| PPy/$[Pd(DMIT)_2]^{2-}$ | 2.3 | 4914.0 | 0.9313 | $4.3 \times 10^{-3}$ |
| PPy/$[Pt(DMIT)_2]^{2-}$ | 2.7 | 3623.9 | 0.9313 | $3.9 \times 10^{-3}$ |
| PPy/$[Sn(DMIT)_3]^{2-}$ | 4.0 | 1647.4 | 0.9313 | $5.6 \times 10^{-7}$ |

Where $f_{12}$ is the finite thickness correction factor, $s$ is the distance between the probes (1.2 mm) and $f_{2R}$ was estimated for an area of 1.0 $cm^2$. $f_{2R}$ is the finite corrections

et al. [67] showed that the size and the geometry of the incorporated counteranion affect the conductivity mechanism of PPy films. Parallel alignment of PPy chains in films is considered to be most important for good conductivity. PPy films containing such anions as $[Bi(DMIT)_2]^-$ and $[Sn(DMIT)_3]^{2-}$ will not have the desired parallel alignment, due to the bulk and shape of these anions. Both anions, $[Bi(DMIT)_2]^-$ [68] and $[Sn(DMIT)_3]^{2-}$ [69], in their tetraalkylammonium salts have distorted octahedral geometries. While, in these salts, discrete $[Sn(DMIT)_3]^{2-}$ dianions are present, $[Bi(DMIT)_2]^-$ anions are linked via inter-anion metal–sulphur interactions. Even if, in the films, the inter-anion Bi–S interactions are broken, the geometry of the $[Bi(DMIT)_2]$ moiety would still be far from planar, having a near tetrahedral geometry, and thus would still obstruct the channels responsible for the interchain charge transport and reduce the overall conductivity.

The nearly planar geometry of $[M(DMIT)_2]^{2-}$ (M = Ni, Pd and Pt) dianions, on the other hand, appears to promote an optimized alignment of the polymer chains, which favours the conductivity mechanism when compared to the PPy/$[Bi(DMIT)_2]^-$ and PPy/$[Sn(DMIT)_3]^{2-}$ materials.

From the data in Table 4, the maximum conductivity values are associated with polymeric materials incorporated with planar counteranions. As shown by Saunders [38], anions with complex chemical structures show low conductivity but great charge capacity. This property is crucial when studying materials for energy storage devices.

## Conclusions

Hybrid materials have been obtained by the electropolymerization of pyrrole using DMIT-containing counteranions. The growth mechanism as well as the influence of the geometry and size of the incorporated couteranion seems to be responsible for the different morphologies. The spectroscopic analysis confirmed the insertion of unmodified DMIT containing counteranions into the polypyrrole backbone. The disappearance of absorption peak assigned to asymmetric stretching of –NH indicates interaction of DMIT moiety with PPy from –NH bond. The electrochemical analysis showed that films are electroactive undergoing redox process related to both PPy and the counteranion. The hybrid films are thermally stable and this stability reflects the stabilities of the incorporated counteranions. All the volume conductivity values were in the range expected for semiconductors, and for the films I, II and III, the insertions of the nearly planar counteranions allow optimized conformational arrangements of the polymeric chains, which appear to be responsible for the values of the conductivities.

**Acknowledgements** The authors thank Capes and CNPq for fellowships, N. M. Comerlato and G. B. Ferreira for supplying the $[NEt_4]_2[Zn(DMIT)_2]$ complex and FAPERJ (Proc. No. E-26/170.700/2004) for financial support.

## References

1. Malinauskas A, Malinauskien J, Ramanavičius A (2005) Nanotechnology 16:R51. doi:10.1088/0957-4484/16/10/R01
2. Lange U, Roznyatovskaya NV, Mirsky VM (2008) Anal Chim Acta 61:41
3. Yamamoto K, Yamada M, Nishiumi T (2000) Polym Adv Technol 11:710. doi :10.1002/1099-1581(200008/12)11:8/12<710::AID-PAT24>3.0.CO;2-K
4. Inzelt G, Pineri M, Schultze JW, Vorotyntsev MA (2000) Electrochim Acta 45:2403. doi:10.1016/S0013-4686(00)00329-7
5. Malinauskas A (2001) Polymer Guildf 42(9):3957. doi:10.1016/S0032-3861(00)00800-4
6. Deslouis C, Duprat M, Tournillon C (1989) Corros Sci 29:13. doi:10.1016/0010-938X(89)90077-2
7. Ferreira CA, Lacaze JC (2001) J Electrochem Soc 148(4):121. doi:10.1149/1.1354613
8. Kesting RE, Fritzsche AK (eds) (1993) Polymeric gas separation membranes. John Wiley & Sons, Inc., New York, USA
9. Guimard NK, Gomez N, Schmidt CE (2007) Prog Polym Sci 32:876. doi:10.1016/j.progpolymsci.2007.05.012
10. Otero TF (1997) In: Nalwa HS (ed) Handbook of organic conductive molecules and polymers, Chapter 10, vol 4. Wiley, Chichester, UK
11. Carter FL (ed) (1982) Molecular electronic devices. Marcel Dekker, New York.
12. Lubentsov BZ, Zvereva GI, Samovarov YH, Bystriak SM, Timofeeva ON, Khidekel MI (1991) Synth Met 41:1143; Krieger YG (1993) J Struct Chem 34:896
13. (a) Otero TF, Villanueva S, Cortes MT, Cheng SA, Vazquez A, Boyano I (2001) Synth Met 119:419. doi:10.1016/S0379-

6779(00)01273-X; (b) Saito Y, Azechi T, Kitamura T, Hasegawa Y, Wada Y, Yanagida S (2004) Coord Chem Rev 248:1469. doi:10.1016/j.ccr.2004.03.025
14. Rowley NM, Mortimer RJ (2002) Sci Prog 85(3):243
15. Wang F, Wilson MS, Rauh RD, Schottland P, Thompson BC, Reynolds JR (2000) Macromolecules 33:2083. doi:10.1021/ma9918506
16. Luna AMC (2000) J Appl Electrochem 30:1137. doi:10.1023/A:1004050922065
17. Bouzek K, Mangold K-M, Jüttner K (2000) Electrochim Acta 46:661. doi:10.1016/S0013-4686(00)00659-9
18. Bargon J, Baumann R (1993) Microelectronic Eng 20:55. doi:10.1016/0167-9317(93)90207-L
19. Ryder KS, Morris DG, Cooper JM (1997) Biosens Bioelectron 8:721. doi:10.1016/S0956-5663(97)00039-0
20. Frommer JE, Chance RR (eds) (1986) Electrically conducting polymers. Encyclopaedia Polym Sci Eng 5:462
21. Saunders BR, Murray KS, Fleming RJ (1992) Synth Met 47:167. doi:10.1016/0379-6779(92)90384-U
22. Wang G, Chen H, Zhang H, Shen Y, Yuan C, Lu Z et al (1998) Phys Lett A 237:165. doi:10.1016/S0375-9601(97)00837-2
23. Saunders BR, Murray KS, Fleming RJ, Korbatieh Y (1993) Chem Mater 5:809. doi:10.1021/cm00030a016
24. Saunders BR, Murray KS, Fleming RJ, McCulloch DG (1995) Synth Met 69:363. doi:10.1016/0379-6779(94)02487-J
25. Pullen AE, Olk R-M (1999) Coord Chem Rev 188:211. doi:10.1016/S0010-8545(99)00031-4
26. da Cruz AGB, Wardell JL, Simão RA, Rocco AM (2006) Electrochim Acta 52:1899. doi:10.1016/j.electacta.2006.07.061
27. da Cruz AGB, Wardell JL, Simão RA, Rocco AM, Rangel MVD (2007) Synth Met 157:80. doi:10.1016/j.synthmet.2006.12.010
28. Pereira RP, Wardell JL, Rocco AM (2005) Synth Met 150:21. doi:10.1016/j.synthmet.2004.12.020
29. da Cruz AGB, Wardell JL, Rocco AM (2006) Synth Met 156:396. doi:10.1016/j.synthmet.2005.12.026
30. Steimecke G, Sieler H-J, Kirmse R, Hoyer E (1979) Phosporous Sulfur 7:49. doi:10.1080/03086647808069922
31. Yu L, Zhu D (1996) Phosporous Sulfur 116:225. doi:10.1080/10426509608040483
32. Malfant I, Cordente N, Lacroix PG, Lepetit C (1998) Chem Mater 10:4079. doi:10.1021/cm980487z
33. Cassoux P, Valade L, Kobayashi H, Clark RA, Underhill AE (1991) Coord Chem Rev 110:115. doi:10.1016/0010-8545(91)80024-8
34. Bates JR, Milesa RW, Kathirgamanathan P (1996) Synth Met 76:313. doi:10.1016/0379-6779(95)03479-4
35. Bates JR, Kathirgamanathan P, Miles RW (1997) Thin Solid Films 299:18. doi:10.1016/S0040-6090(96)09172-9
36. Abruña HD (1988) Coord Chem Rev 86:135. doi:10.1016/0010-8545(88)85013-6
37. Abrantes LM, Correia JP (1999) Electrochim Acta 44:1901. doi:10.1016/S0013-4686(98)00299-0
38. Nalwa HS (ed) (1997) Handbook of conductive polymers: spectroscopy and physical properties, Chapter 12, vol 3. Wiley, Chichester, UK
39. Simon A, Ricco AJ, Wrighton MS (1982) J Am Chem Soc 104:2031. doi:10.1021/ja00371a045
40. Collard DM, Sayre CN (1997) Synth Met 84:329. doi:10.1016/S0379-6779(97)80768-0
41. Takakubo M (1987) Synth Met 16:167. doi:10.1016/0379-6779(86)90109-8
42. Rocco AM, Pereira RP, Bonapace JAP, Comerlato NM, Wardell JL, Milne BF et al (2004) Inorg Chim Acta 357:1047. doi:10.1016/j.ica.2003.09.026
43. Liu G, Fang Q, Xu W, Chen H, Wang C (2004) Spectrochim Acta A: Mol Biomol Spectrosc 60:541. doi:10.1016/S1386-1425(03)00260-9
44. Valade L, Legros J-P, Cassoux P (1986) Mol Cryst Liq Cryst (Phila Pa; 2003) 140:335. doi:10.1080/00268948608080163
45. Pullen AE, Abboud KA, Reynolds JR (1996) Phys Rev B 53:10557. doi:10.1103/PhysRevB.53.10557
46. Jang J, Yoon H (2003) Chem Commun (Camb) 720. doi:10.1039/b211716a
47. Cervini R, Fleming RJ, Murray KS (1992) J Mater Chem 2:1115. doi:10.1039/jm9920201115
48. Han J, Lee S, Paik W (1992) Bull Korean Chem Soc 13
49. Shilabin AG, Entezami AA (2000) Eur Polym J 36:2005. doi:10.1016/S0014-3057(99)00262-1
50. Li F, Albery WJ (1991) J Chem Soc, Faraday Trans 87:2949. doi:10.1039/ft9918702949
51. Cheung KM, Bloor D, Stevens GC (1990) J Mater Sci 25:3814. doi:10.1007/BF00582447
52. Dong S, Lian G (1990) J Electroanal Chem 291:23. doi:10.1016/0022-0728(90)87174-I
53. Varela H, Bruno RL, Torresi RM (2003) Polymer (Guildf) 44:5369. doi:10.1016/S0032-3861(03)00526-3
54. McCormac T, Breens W, McGree A, Cassidy JF, Lyons MEG (1995) Electroanalysis 287
55. Lyons MEG, Breens W, Cassidy JF (1991) J Chem Soc, Faraday Trans 87:115. doi:10.1039/ft9918700115
56. McCormac T, Farrell D (2001) Electrochim Acta 46:3287. doi:10.1016/S0013-4686(01)00621-1
57. Cheng S, Otero TF, Coronado E, Garcia CJG, Ferrero EM, Saiz CG (2002) J Phys Chem B 106:7585. doi:10.1021/jp014340y
58. Bobacka J, Ivaska A, Grzeszczuk M (1991) Synth Met 44:9. doi:10.1016/0379-6779(91)91853-3
59. Cervini R, Fleming RJ, Kennedy BJ, Murray KS (1994) J Mater Chem 4:87. doi:10.1039/jm9940400087
60. Uyar T, Toppare L, Hacaloglu J (2002) J Anal Appl Pyrolysis 64:1. doi:10.1016/S0165-2370(01)00166-8
61. da Cruz AGB, Wardell JL, Rocco AM (2006) Thermochim Acta 443:190
62. Smits FM (1958) Bell Syst Tech J 37:711
63. Uhlir A Jr (1955) Bell Syst Tech J 34:105
64. Zimney EJ, Dommett GHB, Ruoff RS, Dikin DK (2007) Meas Sci Technol 18:2067. doi:10.1088/0957-0233/18/7/037
65. Girotto EM, Santos IA (2002) Quim Nova 25:639. doi:10.1590/S0100-40422002000400019
66. Wernet W, Wegner G (1987) Makromol Chem 188:1465. doi:10.1002/macp.1987.021880621
67. Yamaura M, Hagiwara T, Iwata K (1988) Synth Met 26:209. doi:10.1016/0379-6779(88)90238-X
68. Comerlato NM, Costa LAS, Howie RA, Pereira RP, Rocco AM, Silvino AC et al (2001) Polyhedron 20:415. doi:10.1016/S0277-5387(00)00643-4
69. Fereira GB, Comerlato NM, Wardell JL, Hollauer E (2005) Spectrochim Acta A: Mol Biomol Spectrosc 61:2663